The Development and Validation of In Vivo Optimal Fiber Length Measurement

Tieme B. Arkema

In partial fulfilment of the requirements of

Master of Science

in Biomedical Engineering

Track Neuromusculoskeletal Biomechanics

at the Delft University of Technology, to be defended publicly on

Monday 12-15-2025 at 10:45

Thesis advisors: dr. ir. E. van der Kruk

em. prof. dr. H.E.J. Veeger

Thesis committee: dr. ir. E. van der Kruk[1] (chair)

em. prof. dr. H.E.J. Veeger[1]

dr. ir. M. van de Ruit[1]

[1]BioMechanical Engineering, Biomechatronics & Human-Machine Control, Delft University of Technology

An electronic version of the thesis is available at: https://repository.tudelft.nl/

Abstract

Musculoskeletal modelling forms an important asset in research on understanding human motions and neuromuscular performance. The reliability of musculoskeletal model outcomes depend on the accuracy of the parameters, particularly Optimal Fiber Length (OFL). However, the OFL may vary considerably between populations. To date it is unknown how such variations might affect musculoskeletal modelling. Therefore, in vivo determination of OFL is essential for subject-specific models, and understanding population-specific differences for improvement of model diversity. This study developed an in vivo methodology for measuring the OFL that is easily accessible for large scale implementations. It was applied it to the m. rectus femoris for validation.

OFL was derived from the force-length relationship by measuring muscle force, calculated from knee moments, muscle-tendon moment arm, and fascicle length using ultrasound. Muscle activation was standardized via electrical stimulation. The protocol was separately evaluated for validity, reliability, and usability.

Results indicated that knee moment and muscle-tendon moment arm measurements deviated from literature values due to experimental setup limitation, and active fascicle lengths could not be reliably estimated due to the complex muscle architecture. Consequently, the current approach did not yield valid OFL estimates. This study provides insight into the challenges of developing reliable in vivo measurement techniques.

Future studies should employ improved experimental approaches such as increasing electrical muscle stimulation, use of dynamometry and more advanced ultrasound techniques, and applications to other muscles and joints, ultimately, providing a foundation for in vivo estimation of OFL, facilitating investigation of population-specific differences and improving diversity in musculoskeletal modelling.

1. Introduction

Musculoskeletal modelling forms an important asset in research on understanding human motions and neuromuscular performance (Wakeling et al., 2023). Musculoskeletal models represents the muscular and skeletal characteristics, enabling the estimation of the muscle forces and joint moments required for body movements. The muscle forces are typically determined using a Hill-type muscle model that is parameterised with the optimal fiber length (OFL), physiological cross-sectional area (PCSA), tendon slack length, tendon stiffness, width, force-velocity parameters (Hill, 1938; Pandy and Zajac, 1991; van Soest & Bobbert, 1993). The reliability of Hill-type muscle model outcomes depend on the accuracy of the parameters, particularly the tendon slack length and OFL in simulations of walking and running (Scovil and Ronsky, 2005; Redl et al., 2007; De Groote et al., 2010). However, muscle parameters may vary considerably between individuals, age-groups, sexes and demographic populations (Brand et al., 1986 and Friedrich and Brand, 1990). To date it is unknown how such variations might affect musculoskeletal modelling. Therefore, individual parameter estimation is essential for subject-specific models, and gaining insight into population-specific differences in muscle parameters is necessary to improve model diversity.

Most biomechanical studies scale open-source gen eric musculoskeletal models, such as those in OpenSim (Delp et al., 2007) and Anybody (Damsgaard er al., 2006), for individual parameter estimation. The OFL is commonly scaled with segment length. Generic musculoskeletal model often rely on limited datasets from cadaveric studies, which is suboptimal because it might poorly reflects in vivo muscles properties and population-specific variability. In addition, previous research has demonstrated that the OFL exhibits a weak linear relationship with segment length (Ward et al., 2005; 2007; Charles et al, 2019), and such scaling approaches of the OFL perform poorly in gait-simulation studies (Luis et al., 2022). Consequently, a method for in vivo, individual measurement of OFL is necessary. For investigation of population-specific differences, the method must be easily accessible to allow implementation across large cohorts.

The OFL is defined as the muscle fiber length at which they can produce maximal isometric force (Fmax). This property arises from the force-length relationship, as described by the sliding filament theory (Abbott & Aubert, 1952; Gordon et al., 1966). Muscle fibers consist of contractile units called sarcomeres, that are made of actin and myosin filaments. As a muscle shortens or lengthens, the filaments slide along each other and the amount of overlap between the filaments determines the amount of crossbridges that can be made (Gordon et al., 1966). More crossbridges means more force and there is a maximal amount of overlap that results in maximal force. The sarcomere length at maximal overlap is the optimal sarcomere length (Gordon et al., 1966; Walker & Schrodt, 1974). Since a muscle fiber is composed of series of sarcomeres, a muscle fiber too has an optimal length, known as OFL. A maximally activated muscle produces Fmax at optimal fiber length. The force-length relationship forms an inverted hyperbola parameterised with the OFL, Fmax and width of the hyperbola.

Several in vivo methods for determination of OFL have been developed based on direct measurement of sarcomere length including micro-endoscopy (Adkins et al., 2021; Lichtwark et al., 2018; Chen & Delp, 2016; Cromie et al., 2012), resonant reflection spectroscopy (Young et al., 2017) or intraoperative laser diffraction (Lieber et al., 1994). These techniques provide precise in vivo sarcomere length measurements during dynamic contractions, enabling OFL estimation from fascicle length and optimal sarcomere length. Although these approaches offer valuable insight into in vivo sarcomere behaviour, they remain invasive, technically demanding and expensive, limiting their accessibility and current applicability to measure individual OFL.

Other methods for in vivo determination of OFL have been established (Maganaris, 2001; Nikolaidou et al., 2017; Yu & Herzog, 2023; Mornas et al., 2024a). These protocols combine ultrasonographic assessment of fascicle length and pennation angle, dynamometric measurement of joint moment, and estimation of the muscle-tendon moment arm via MRI or regression. From these data, muscle force and fascicle length are derived, enabling characterization of the muscle force-length relationship and subsequent OFL determination. To avoid an effect of muscle activity, consistent muscle activation across measurements is ensured through electrical muscle stimulation or maximal voluntary contractions (MVC). The OFLs have been reported of the m. tibialis anterior [5.5 cm], m. soleus [3.5 cm] (Maganaris, 2001), m. gastrocnemius medialis [6.2 cm] (Mornas et al., 2024a) and mm. vastii [9.4 cm and 9.4 cm] (Nikolaidou et al., 2017; Yu & Herzog, 2023) and show correspondence with other values reported in literature, indicating the validity of their results (cadaveric studies (Horsman et al., 2006; Ward et al., 2008), optimisation and nonlinear scaling studies (Hasson and Caldwell, 2012; Winby et al., 2008; Modenese et al., 2016))

Nonetheless, the above mentioned studies show notable inconsistencies in the measurement of the muscle-tendon moment arm, computational muscle model, and muscle activation methods. Maganaris (2001) did not define the joint rotation centre in assessing muscle-tendon moment arm and applied an incorrect computational muscle model (Hoffman et al. (2012), reducing the reliability of the derived OFL. Regression-based moment-arm estimates used by Mornas et al. (2024a) and Yu and Herzog (2023) improve consistency but remain less precise than direct measurements. Additionally, MVCs in Yu and Herzog (2023) and Nikolaidou et al. (2017) produced forces from entire muscle groups rather than individual muscles, invalidating muscle-specific OFL values and underscoring the necessity of electrical muscle stimulation for muscle-specific activation.

The aim of this study was to develop and test an in vivo methodology for OFL measurement, facilitating the investigation of population-specific differences for improving diversity and development of subject-specific models. Hence, the method must be in vivo and easily accessible for implementation on a large populations. Subsequently, the validity and reliability were tested in the OFL measurement of the m. rectus femoris. The knee joint is an optimal site for OFL measurement due to its mechanical simplicity: subtraction of passive force-length relation is unnecessary, the rotation axis is well defined, and motion and joint moments occur predominantly about a single axis. Moreover, activation of the m. rectus femoris yields a uniform force distribution in the patellar tendon, minimizing asynchronous loading.

2. Method

This study aimed to develop and validate an experimental method for determining the OFL of an in vivo muscle. The m. rectus femoris was used as a test muscle to implement and evaluate the proposed protocol. The OFL was derived from the muscle's force-length relationship, obtained by simultaneously measuring muscle force and fascicle length at different knee angles. Muscle force was calculated by dividing the total knee joint moment by the muscle-tendon moment arm, measured using motion capture and an one-dimensional loadcell. Fascicle length was measured using ultrasound synchronized in time with the motion capture system. At each joint position, the muscle was activated using electrical muscle stimulation to ensure consistent activation across measurements. The proposed methodology contains four parts: (2.1) *electrical muscle stimulation*, (2.2) *the measurement of muscle-tendon moment arm*, (2.3) *the measurement of knee moment and muscle force* and (2.4) *the measurement of fascicle length*. Each part was evaluated in separate experiments (2.1, 2.2, 2.3, 2.4) for validity, reliability and usability.

Participant	Sex	Age	Height (cm)	Weight (kg)	Experiment
A	Male	24	181.1	72.1	2.1, 2.2, 2.3 2.4
B	Female	24	172.0	68.9	2.2, 2.3
C	Female	21	167.0	56.1	2.2
D	Male	24	180.5	72.9	2.1

Table 1: Participant information and in which experiments they participated

2.1 Electrical Muscle Stimulation

Equal muscle activation across measurements is essential when establishing the force-length relationship. This was achieved using submaximal electrical muscle stimulation, delivered via surface electrodes. A protocol for applying electrical muscle stimulation was developed to ensure reproducibility and participant safety. The aim of experiment 2.1 was to evaluate the reliability and applicability of electrical muscle stimulation by assessing the consistency of the evoked force response and examining the suitability of electromyography (EMG) for detecting activity in surrounding muscles by applying a notch filter at the electrical muscle stimulation frequencies and its harmonics.

2.1.1 Materials and method

2.1.1.1 Electrical muscle stimulation protocol

Electrical muscle stimulation of the m. rectus femoris was induced using Micromed ENERGY stimulator (Micromed, Mogliano Veneto, Italy). Two electrodes were placed on the muscle, a proximal electrode on the most proximal palpable part of the muscle and a distal electrode approximately 2 cm proximal to the point where the muscle passes beneath the mm. vastus lateralis and medialis. Participants were instructed to remain relaxed during stimulation and the stimulation parameters were not changed during the experiment.

Stimulation parameters were individualized to maximize force while minimizing fatigue and discomfort. Each measurement used a 3 s stimulation to reach force equilibrium, with optimal settings identified within five test stimulations. Frequency was set at 80 Hz and reduced to 60 Hz if discomfort occurred. Current was increased from 15 to 50 mA, with the highest tolerable non-fatiguing current selected.

2.1.1.2 Experimental protocol

Consistency of electrical muscle stimulation was evaluated by investigating the variability in force responses under constant stimulation parameters and knee angle. Force responses were recorded from participant D (table 1) using a one-dimensional loadcell (SCAIME SAS, Annemasse, France) connected to a cord that was attached to the ankle, fixation the knee angle. Stimulation was delivered at 60 Hz, 3 s duration, and 37 mA, repeated ten times with five-minute rest intervals.

The suitability of surface EMG for detecting adjacent muscle activity during stimulation was examined in participant A (table 1). EMG electrodes were positioned on the m. vastus medialis according to SIAM guidelines. EMG signals were recorded in millivolts using the Delsys Trigno Wireless EMG System (Delsys Inc., Boston, MA, USA) at 2000 Hz. Two conditions were tested, (1) electrical stimulation followed by voluntary activation producing matched force, and (2) electrical stimulation during voluntary activation. Stimulation was delivered at 60 Hz, 3 s duration, and 35 mA.

2.1.2 Data Processing

The peak force response for each electrical muscle stimulation was obtained and mean and standard deviation were calculated. EMG-signals were band-pass filtered (25-500 Hz, second-order Butterworth filter) and rectified as standard processing step. Subsequently, a fourth order notch Butterworth band-stop filter with bandwidth of 10 Hz was applied at the frequency of the electrical stimulation and its harmonics to compare to the standard EMG-signal. All processing steps were performed in MATLAB (MathWorks, Natick, MA, USA).

2.1.3 Results

Figure (1) shows good consistency of the force response over time, mean force response was 67.45 (3.44) N. In figure (2a) can be seen that the amplitude of the electrical muscle stimulation is not completely filtered out, while the voluntary signal remains relatively unchanged. Figure (2b) shows the same as the EMG-signal remains elevated after filtering during the electrical muscle stimulation.

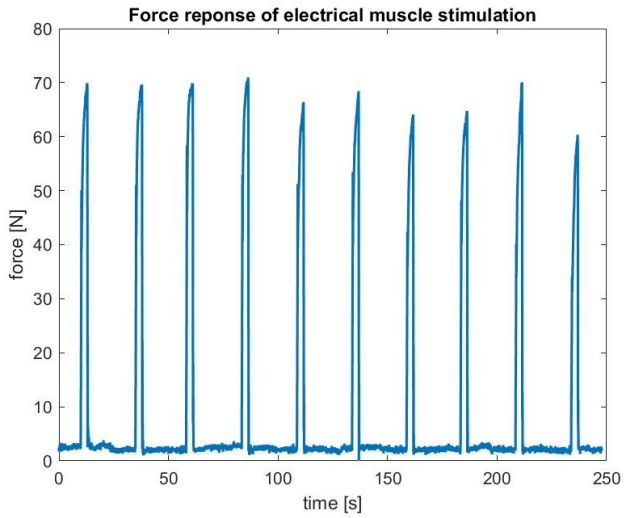

Figure 1: The force response of 10 electrical muscle stimulations (with 5 minutes rest, not shown) measured with a loadcell. Stimulation parameters (3 sec, 60 Hz, 37 mA) and knee angle were constant. Sample frequency of 20 Hz and data in between stimulation not shown. The mean peak force response was 67.45 (3.44) N.

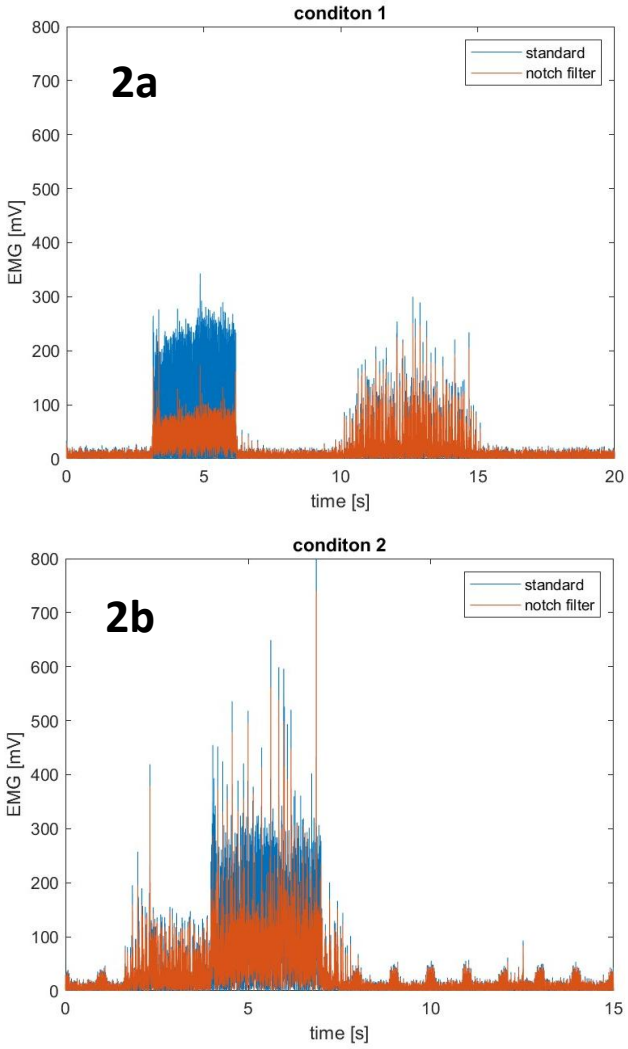

Figure 2: a: EMG-signal of m. vastus medialis condition 1: electrical muscle stimulation followed by voluntary activation. b: EMG-signal of m. vastus medialis condition 2: electrical muscle stimulation during voluntary activation. Legend: standard: bandpass filtered 25-500 Hz and rectified, notch filtered: notch filter at stimulation frequency and harmonics. Stimulation parameters were 3 sec, 60 Hz, 35 mA.

2.2 The Measurement of Muscle-tendon Moment Arm

When calculating the muscle force, the muscle-tendon moment arm is required. The muscle-tendon moment arm was obtained with the excursion method. The aim of experiment 2.2 was to assess the validity and reliability of the muscle-tendon moment arm by applying the excursion method to the m. rectus femoris. The excursion method determines the muscle-tendon moment arm as function of joint angle by dividing the change of muscle-tendon-unit length by the change of joint angle (Fick, 1910, p305).

$$r_{m.\ rf}(\varphi_{knee}) = \frac{dL_{m.rf}}{d\varphi_{knee}} \qquad (1)$$

In which $r_{m.\ rf}(\varphi_{knee})$ represents the muscle-tendon moment arm of the m. rectus femoris as function of the knee-angle (φ_{knee}). $dL_{m.rf}$ is the change of muscle-tendon-unit length and $d\varphi_{knee}$ is the change of knee-angle.

2.2.1 Materials and Method

The muscle-tendon moment arm was obtained from participants A, B and C (table 1), during active extension in which they extended the knee from 110° to 0° (0° indicated a straight leg). Clusters of three reflective markers were attached to the thigh and shank. Anatomical landmark positions (trochanter major, lateral and medial femoral epicondyles, and lateral and medial malleoli) were obtained relative to the clusters using a pointer device equipped with three reflective markers, with the tip location known in the pointer coordinate system. The position of lig. patellae was identified midway between the apex patellae and tuberositas tibiae and was tracked with the pointer during the extension, see appendix (I) on how this point was selected. Reflective marker positions were measured using a Qualisys motion capture system (Qualisys, Gothenburg, Sweden). Three separate extensions were recorded per participant.

2.2.2 Data Processing

Data processing steps were performed in MATLAB. $r_{m.\ rf}(\varphi_{knee})$ was calculated in millimetres using equation (1), with $d\varphi_{knee}$ and $dL_{m.rf}$ obtained by differentiating φ_{knee} and $L_{m.rf}$ over time. φ_{knee} was calculated using the positions of the anatomical landmarks relative to the clusters during the extension, see appendix (II). $L_{m.rf}$ was obtained as the norm of the lig. patellae position vector relative to the last 0.5 sec as the knee was fully extended. Both $d\varphi_{knee}$ and $dL_{m.rf}$ were low-pass filtered (4th-order Butterworth, 1 Hz cutoff) to reduce noise from differentiation. Samples with angular velocities below 0.15 rad/s were excluded to minimize noise and to avoid filtering-related boundary artefacts.

2.2.3 Results

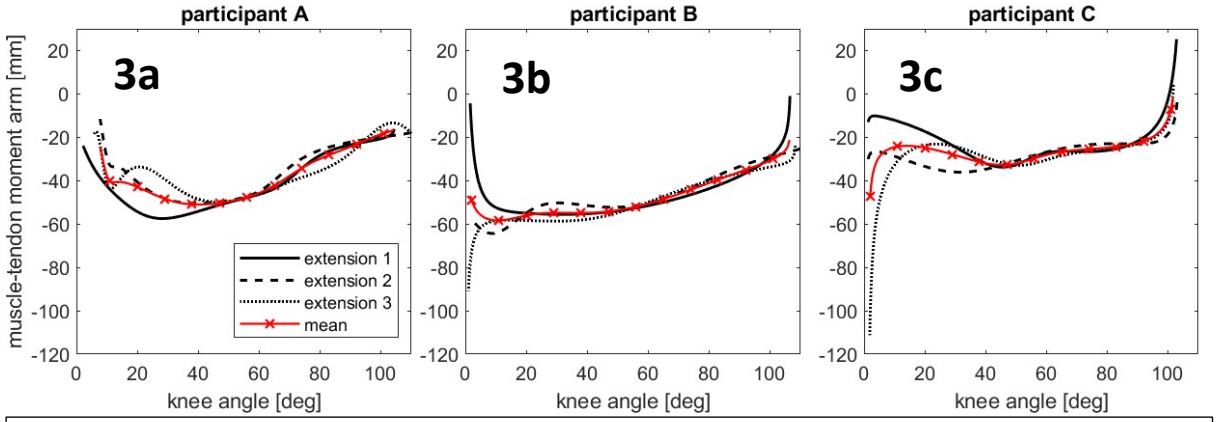

Figure 3: Muscle-tendon moment arm in millimetres as function of knee angle in degrees of participants A (3a), participant B (3b) and participant C (3c) . For participant three separate measured extensions (1, 2 & 3) and the average muscle-tendon moment arm of . 0° indicated a straight leg.

Figure (3a, 3b and 3c) shows pronounced variations of muscle-tendon moment arm within participants near small and large knee angles (<20°and >95°) as values range between -110 mm (participant C, extension 3) and 20 mm (participant C, extension 1). These variation may reflect a reduced signal-to-noise ratio. For intermediate knee angles, the muscle-tendon moment arm shows good within-participant consistency. Between-participant variation can be observed, highlighting the inter-individual differences.

2.3 The measurement of Knee Moment and Muscle Force

The aim of experiment 2.3 was to develop and evaluate a method for measuring the knee joint moment and calculating the corresponding m. rectus femoris force. The knee moment was measured at five

knee angles and the muscle force was calculated with the muscle-tendon moment arm corresponding to the knee angle.

2.3.1 Materials and method

Knee moments were assessed in participants A and B (Table 1). The participants were seated in a chair according figure (4), with an adjustable leg-rest to ensure isometric contractions. Targeted knee angles were set with a manual goniometer and fixated using an ankle-mounted cord (0^o indicated a straight leg). Hip angle was fixated with a strap band. The positions of anatomical landmarks (trochanter major, lateral and medial femoral epicondyles, and lateral and medial malleoli) were obtained relative to the clusters using the pointer device. During simultaneous collection of marker positions with Qualisys and cord force with the loadcell submaximal muscle activation was induced via electrical muscle stimulation (see 2.1.1.1). Measurements were performed three times at five knee angles (0°, 20°, 40°, 60°, 90°) presented in random order.

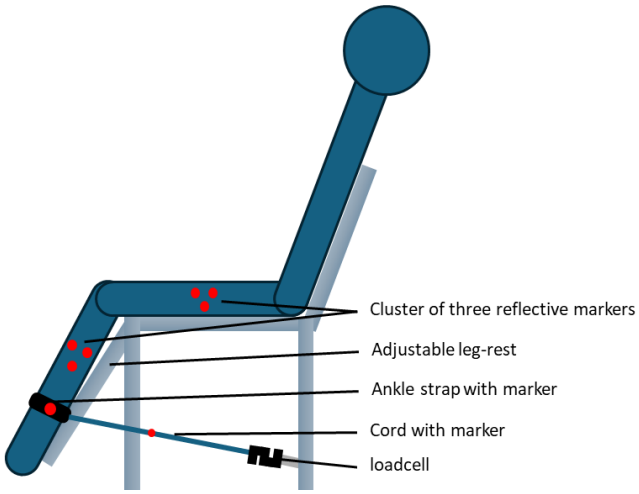

Figure 4: Experimental setup of knee moment measurement. Labelled elements are indicated with the black lines. Clusters of three reflective markers were attached to the thigh and shank. Additional reflective markers were placed on the ankle and cord to obtain the direction of the cord force.

2.3.2 Data processing

The knee moment was calculated using moment-equation of the shank, see appendix (III) for full description and free body diagram. The muscle force is calculated with equation 2:

$$F_{m.\,rf} = \frac{\|\bar{M}_{knee}\|}{r_{m.rf}} \qquad (2)$$

In which $F_{m.\,rf}$ denotes the m. rectus femoris force, $\|\bar{M}_{knee}\|$ the norm of the knee moment ($\|\_\|$ denotes the norm of the vector), and $r_{m.rf}$ the muscle-tendon moment arm of the m. rectus femoris as obtained in 2.2. The knee angle for each measurement was computed using the positions of the anatomical landmarks as described in appendix (II). Maximal knee moment and muscle force were determined using a 0.5 s moving average. Data processing steps were performed in MATLAB.

2.3.3 Results

Figure 5 shows the m. rectus femoris force and knee moment as functions of knee angle for participant A and participant B. Although the measured knee angles deviated from the target values, within-angle variability was low due to consistent cord-length settings. Participant A demonstrated high consistency in both knee moment and muscle force across knee angles (Figures 5a and 5b). Muscle force increased

with increasing knee angle, and the maximal knee moment occurred at approximately 45°, reaching about 15 Nm.

In contrast, participant B exhibited greater variability across measurements (Figures 5c and 5d). No systematic increase in muscle force with knee angle was observed. The maximal knee moment was difficult to determine due to one apparent outlier at 60° knee angle, but the data point was retained because no experimental error could be identified.

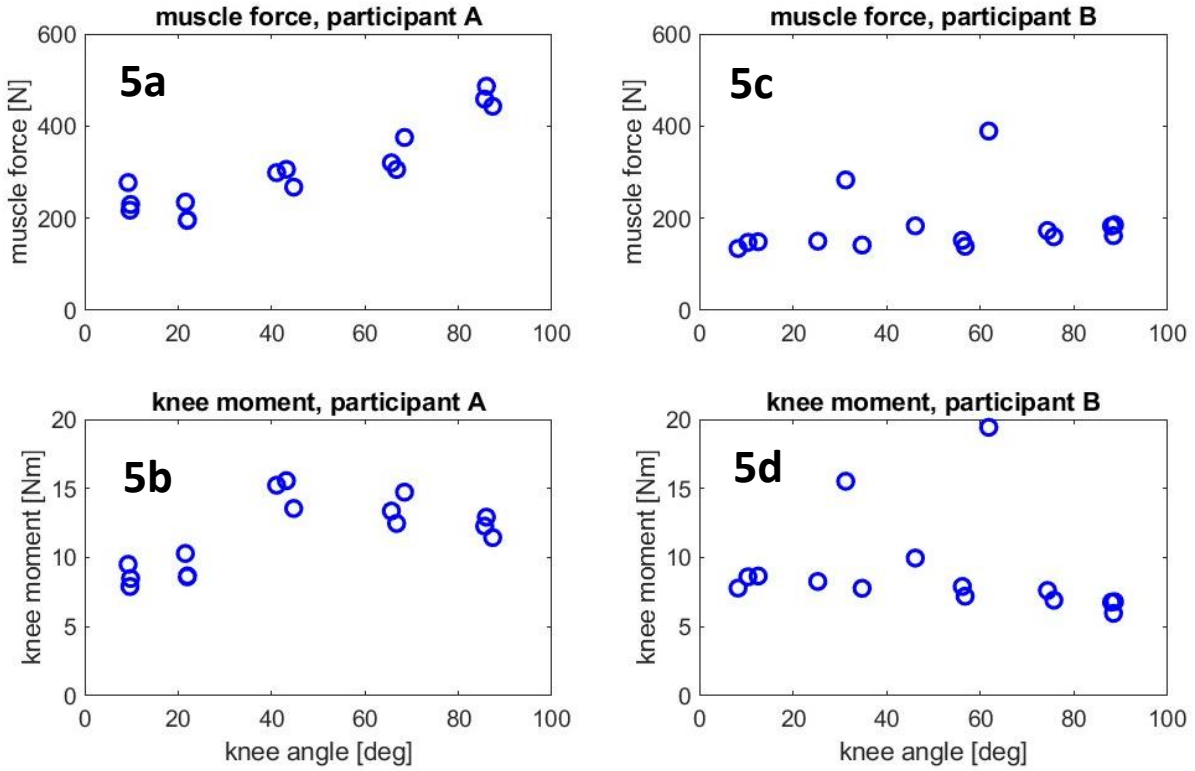

Figure 5: 5a: measured muscle force per measured knee angle for participant A. 5b: measured knee moment per measured knee angle for participant A. 5c: measured muscle force per measured knee for participant B. 5d: measured knee moment per measured knee angle for participant B. 0° indicated a straight leg. At each knee angle the knee moment and muscle force were obtained three times, total 15 measurements per figure represented by the blue circles.

2.4 The Measurement of Fascicle length

The measurement of fascicle length comprised three steps. (1) measurement of relaxed fascicle length, (2) measurement of angle-specific relaxed fascicle length, and (3) measurement of active fascicle shortening during electrical muscle stimulation. Relaxed fascicle length of the m. rectus femoris was obtained from a two-dimensional reconstruction of an ultrasound video acquired during probe sweep from origin to insertion (12-3 MHz linear probe; Philips, Eindhoven, The Netherlands), calibrated and temporally synchronized with the Qualisys motion capture system. Experiment 2.4 aimed to assess the validity and reliability of the relaxed fascicle length measurement.

2.4.1 Experimental Procedure

2.4.1.1 Calibration

For 2D image reconstruction, the transformation of the video-frame with respect to the ultrasound-probe was required. A cluster of three reflective markers was attached to the probe, which was held in a water container, along with the pointer device and an iron rod with a bevelled tip visible in the ultrasound images. Three ultrasound images were captured with the iron rod oriented differently

relative to the probe, while recording the positions of the reflective markers on the probe and pointer. The rod tip was identified in all images to construct a transformation matrix with its basis in the video-frame (${}^{video}_{\diamond}T$). Using the pointer position, a second transformation matrix was defined with its basis in the probe reference frame, defined by the cluster (${}^{probe}_{\diamond}T$). Combining these matrices yielded the transformation from the video-frame to the probe frame, enabling reconstruction of probe movement.

$${}^{probe}_{\diamond}T_{video} = {}^{probe}_{\diamond}T \cdot inv({}^{video}_{\diamond}T) \quad (3)$$

In which the ${}^{probe}_{\diamond}T_{video}$ represents the transformation matrix from video-frame to probe.

2.4.1.2 Synchronisation

Determining probe displacement between video-frames required temporal synchronization of the ultrasound and motion capture systems. At the start and end of the sweep, the probe was pressed against the skin, producing motion artifacts detectable in both systems. These time points were manually identified and used to temporally align the data. The motion capture data was interpolated to match the framerate of the ultrasound video.

2.4.1.3 Two-Dimensional Image Reconstruction

Probe displacement during the sweep was tracked with the cluster of reflective markers in the global reference frame. ${}^{probe}_{\diamond}T_{video}$ was then used to express the video-frame movement in the global reference frame over time.

$${}^{global}_{\diamond}T_{video}(t) = {}^{global}_{\diamond}T_{probe}(t) \cdot {}^{probe}_{\diamond}T_{video} \quad (4)$$

In which ${}^{global}_{\diamond}T_{video}(t)$ and ${}^{global}_{\diamond}T_{probe}(t)$ represent the movement of the video-frame and probe, respectively, in the global reference frame over time. The image was reconstructed with respect to the orientation of the first video-frame as it represented the sweep-plane. Frame displacement was estimated with the mean displacement of the video-frame vertices.

$${}^{video1}_{\diamond}\bar{r}_{vertices}(t) = inv\left({}^{global}_{\diamond}T_{video}(1)\right) \cdot {}^{global}T_{video}(t) \cdot {}^{video}\bar{r}_{vertices} \quad (5)$$

With ${}^{video}\bar{r}_{vertices}$ representing the mean coordinates of the video-frame vertices and ${}^{video1}_{\diamond}\bar{r}_{vertices}(t)$ representing their displacement in the reference frame of the first video-frame over time. Finally, frame displacement was calculated from the x- and y-coordinates using the mm-to-pixel ratio, as z-direction movement was perpendicular to the sweep plane.

$$disp(t) = \frac{1}{mm\ to\ pixel\ ratio} \cdot \sqrt{{}^{video1}_{\diamond}\bar{r}_{verdices,x}(t)^2 + {}^{video1}_{\diamond}\bar{r}_{verdices,y}(t)^2} \quad (6)$$

In which $disp(t)$ denotes the displacement in pixels of each frame and $mm\ to\ pixel\ ratio$ the millimetre-to-pixel ratio, see figure (6) for explanation.

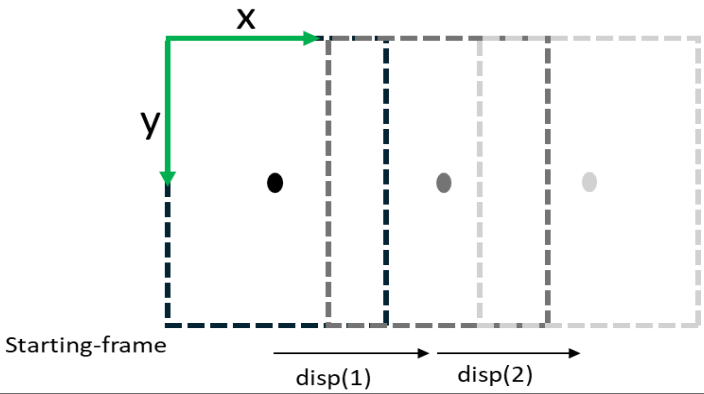

Figure 6: Visualization of frame displacement. The black dotted rectangle represents the first frame and the green arrows represent the x and y axis of its reference frame. With respect to this reference frame, the displacement of subsequent video-frames is calculated. The dark and light grey rectangles represent the second and third video-frame that are displaced with disp(1) and disp(2), respectively.

2.4.1.4 Angle-specific Relaxed Fascicle Length

The probe was mounted in a custom stabilizer fixed to the thigh (figure 7) to image m. rectus femoris distal aponeurosis displacement, which was manually converted using the millimetre-to-pixel ratio. Clusters of reflective markers was attached to the thigh and shank, and anatomical landmark positions (trochanter major, femoral epicondyles, malleoli) were obtained relative to the clusters using a pointer device. The knee was passively flexed from 0^o to 100^o (0^o indicated a straight leg) while aponeurosis displacement and marker positions were recorded. The knee angle was calculated using the position of the anatomical landmarks with respect to the clusters, as described in appendix (II). The angle-specific relaxed fascicle length was derived by adding the relaxed fascicle length obtained from the reconstructed image.

2.4.1.5 Active Fascicle Length

The probe was mounted in a custom stabilizer fixed to the thigh to image the distal aponeurosis of the m. rectus femoris, see figure (7a, 7b). During electrical muscle stimulation from the knee moment measurement (2.3.1), aponeurosis shortening was measured and manually converted using the millimetre-to-pixel ratio. Active fascicle length was calculated by subtracting the shortening from the angle-specific relaxed fascicle length.

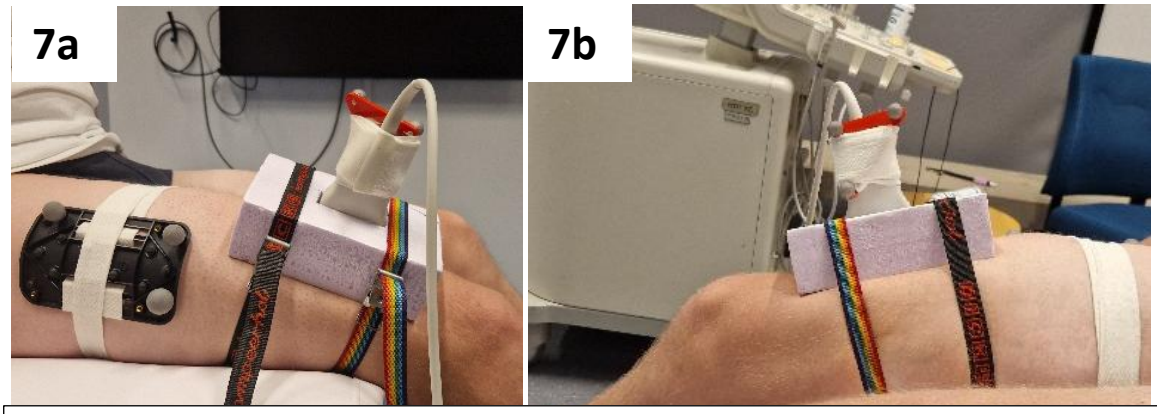

Figure 7a and 7b: Ultrasound probe with probe-stabiliser fixed to the thigh with strap-bands. Clusters of reflective markers are fixed to the thigh (7a) and probe (7a and 7b). Used during measurement of angle-specific relaxed fascicle length and active fascicle length.

2.4.1.5 Validation Experiments

The validity and reliability of the calibration, synchronization, and 2D image reconstruction were evaluated by measuring an iron rod of known length (92.5 mm). The rod was submerged in a container with water, the probe, mounted in the stabilizer, was swept across the container while ultrasound video and marker positions were recorded. The 2D image was reconstructed and the rod length was manually extracted using the millimetre-to-pixel ratio. Six repetitions were performed, and the mean and standard deviation were calculated.

The validity and reliability of the relaxed fascicle length measurement were assessed in participant A (table 1). Three separate probe sweeps were carried out with the leg fully extended (0^o knee angle), and four fascicles across the entire muscle were manually identified per image. Fascicle lengths were calculated in millimetres using the millimetre-to-pixel ratio. The displacement of the video-frame perpendicular to the sweep-plane was visualised to assess the ability to carry out the sweep in a single plane.

2.4.2 Results

Table 2	**Measurement**						
	1	2	3	4	5	6	Mean (SD)
Rod length (mm)	97	96	95	95	94	96	95 (1)

Table 2: resulting lengths of six repeating measurement of iron rod were performed and the mean and standard deviation

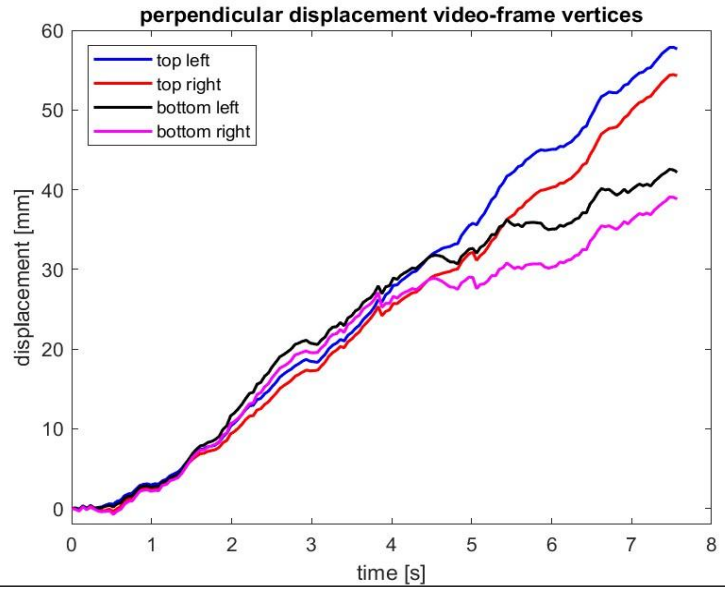

Figure 8: The displacement of the video-frame vertices perpendicular to the sweep-plane. Perpendicular displacement is ideally zero for 2D image reconstruction.

The mean reconstructed rod length was 95 (1) mm, indicating an average overestimation of 2 mm (table 2). All six measurements overestimated the true length, revealing a systematic error in the procedure. As shown in figure 8, the probe sweep did not remain within a single imaging plane, as evidenced by non-zero perpendicular displacement of the video-frame vertices. The probe deviated by approximately 60 mm, and differences in vertex trajectories indicate probe-rotation. Figure 9 provides a reconstructed image of the m. rectus femoris, illustrating how fascicles were identified across the muscle length. Table 3 presents the relaxed fascicle-length measurements from the three probe sweeps, showing variation of fascicles along the muscle, with the greatest lengths observed in the most distal fascicle (fascicle 4).

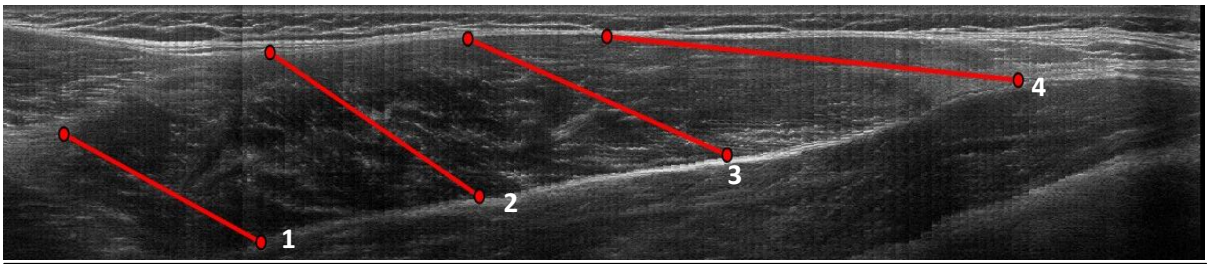

Figure 9: Example of reconstructed image of m. rectus femoris (probe sweep 3). The origo is visible at far left of the image and the insertion into the lig. patellae at the right. In the left top corner, a part of the m. sartorius is visible and from the bottom to the right a large part of the m. vastus intermedius can be seen. The numbered red lines indicate the identified fascicles and were used to calculate their length.

Table 3	Fascicle length (mm)			
	Fascicle 1	Fascicle 2	Fascicle 3	Fascicle 4
Probe sweep 1	77	72	73	100
Probe sweep 2	65	50	64	88
Probe sweep 3	59	63	67	105

Table 3: m. rectus femoris fascicle lengths in millimetre, obtained from three separate probe sweeps. Four fascicles across the entire muscle were identified per reconstructed image from a sweep. The knee was fully extended during each sweep.

3. Discussion

The aim of this study was to investigate the validity and reliability of an in vivo methodology for measuring the OFL, facilitating investigation of populations-specific differences and subject-specific modelling. The methodology consisted of four parts, which were separately investigated. While partial validity was demonstrated, substantial improvements are required before OFL can be confidently determined.

3.1 Electrical Muscle Stimulation

Experiment 2.1 aimed to assess the consistency of electrical muscle stimulation and the suitability of EMG to investigate surrounding muscle activity. The electrical muscle stimulation demonstrated good consistency, as reflected by the small standard deviation in peak force responses (figure 1). The increased variability observed near the end of the protocol (figure 1) may indicate the onset of fatigue, although this finding is based on a single participant and may therefore also reflect random variation. EMG has been shown to be unsuitable for assessing surrounding muscles activity, as the EMG-signals were dominated by stimulation-induced interference, shown in condition 1 and 2 (figure 2a & 2b). The notch filter did not resolve this issue as voluntary activation and stimulation-induced EMG-signals remained indistinguishable (figure 2a & 2b). Furthermore, because the participant was instructed to remain relaxed, it is uncertain whether any voluntary activation would have been present. Stimulation artefacts may also have propagated across the skin to the EMG-electrodes, preventing reliable assessment of muscle activity at all. Although these results are based on a single participants, substantial inter-individual variability is not expected.

3.2 The measurement of muscle-tendon moment arm.

The purpose of experiment 2.2 was to investigate the validity and reliability of the muscle-tendon moment arm measurement. The resulting muscle-tendon moment arms (figure 3a, 3b and 3c) showed substantial variability at small and large knee angles ($<20^{o}$ and $>95^{o}$), even yielding positive values. This is likely due to reduced signal-to-noise ratios at low angular velocities, therefore invalidating muscle-tendon moment arm in this range. Outside these extremes, the moment arms aligned with the shape and range (-10 to -60 mm) reported by Chen and Franklin (2025) (figure 10a, 10b and 10c), supporting the method's validity. Nonetheless, considerable within-participant variability remains suggesting that calculating the mean across repeated measurements may improve the estimates, as illustrated by figure (3a), (3b) and (3c),. Additionally, increasing angular velocity during the measurement might increase validity at small and large knee angles. It should also be noted that the measured moment arm largely reflects the lig. patellae, as patellar displacement was recorded during activation of the entire mm. quadriceps. This limits the ability to calculate solely m. rectus femoris force. However, data reported by Chen and Franklin (2025) indicate that the their moment arms of the m. rectus femoris and lig. patellae are comparable (figure 10a and 10b). Despite involving only three participants, the present findings indicate that the excursion method yields valid estimates when angular velocity is sufficiently high with averaging across multiple measurements.

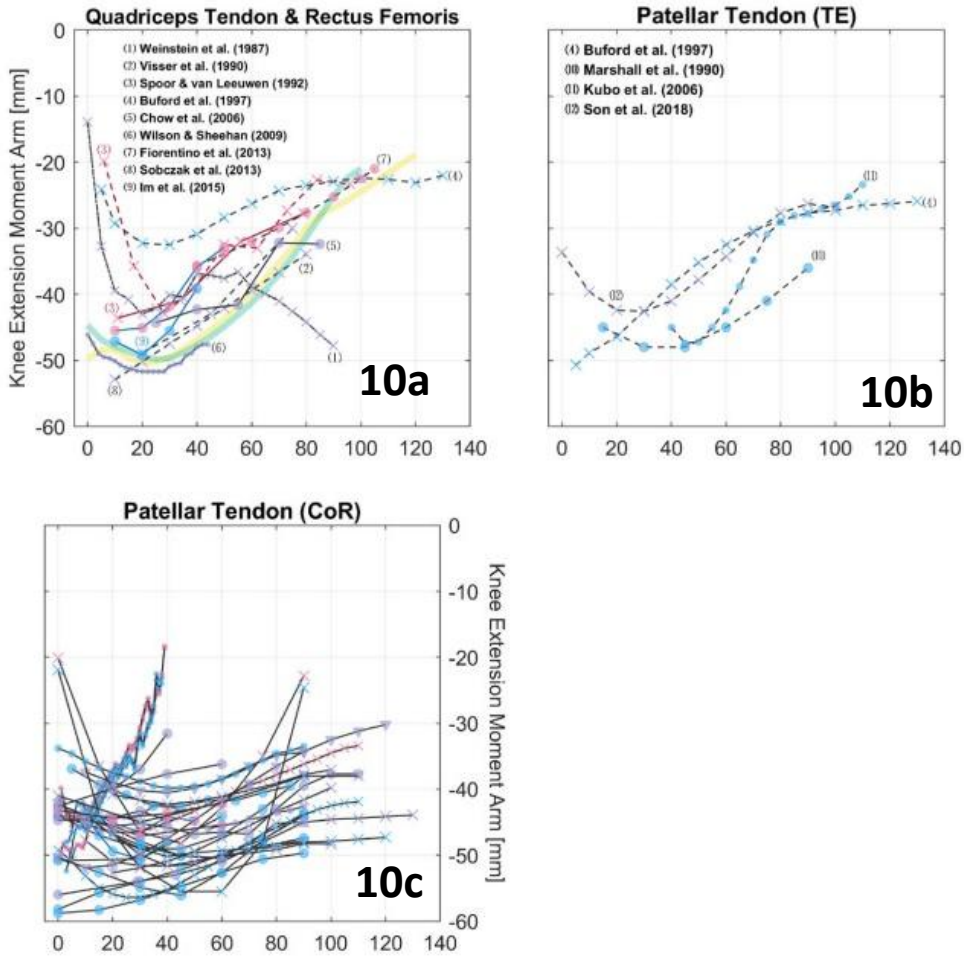

Figure 10: Results for muscle-tendon moment arm. Adapted from Chen and Franklin (2025), who reviewed 35 studies about measuring muscle-tendon moment arm with different methods. a: muscle-tendon moment arm from mm. quadriceps and m. rectus femoris. b: muscle-tendon moment arm lig. patellae obtained with excursion method (TE). c: muscle-tendon moment arm lig. patellae obtained from MRI images as distance to centre of rotation (CoR).

3.3 The measurement of knee moment and muscle force

The aim of experiment 2.3 was to develop and evaluate a method for measuring the knee joint moment and calculating m. rectus femoris force. The calculated knee angle deviated from the targeted knee angle (figure 5), indicating that presetting the knee angle with a manual goniometer is unreliable.

The knee moment-angle relationships obtained (figure 5) deviate from literature, where maximal knee moment occurs around 70^{o} knee angle (Marginson & Eston, 2001; de Ruiter et al., 2004; Kukic et al., 2022), whereas the present study finds a maximum around 30^{o}. This discrepancy arises from the experimental setup: when the shank does not lift off the leg rest, the leg-rest contributes to the measured moment, particularly near small knee angles (<40^{o}) where gravitational moments are large, leading to an overestimation of knee moment. The leg rest prevented excessive knee extension during activation by presetting the knee angle, thereby ensuring isometric contractions and avoiding force alterations due to the force-velocity relationship.

As a consequence, the resulting muscle forces are also invalid (figure 5). As shown by equation 2, their validity depends on both the knee moment and the muscle-tendon moment arm, the latter being unreliable at small and large knee angles, which further reduces validity. Removing the leg-rest could overcome the experimental setup limitation but compromises the assumption of isometric contraction. Increasing electrical muscle stimulation may also help but risks fatigue, potentially reducing force in

later measurements. Alternatively, knee moments could be measured more reliable with a dynamometer, although reducing the accessibility. Together with improved muscle-tendon moment arm estimation, as outlined above, these refinements would enhance muscle force measurements too.

3.4 The measurement of fascicle length

Experiment 2.4 aimed to assess the validity and reliability of fascicle length measurement. The protocol included measurements of relaxed fascicle length, angle-specific relaxed fascicle length, and active fascicle length. Due to time constraints, only the validity of relaxed fascicle length was evaluated. The iron rod measurement showed a small but consistent overestimation of 2 mm (table 2), indicating precision but a systematic error in calibration, synchronisation or reconstruction. In addition, deviations from a single-plane sweep during image acquisition, evidenced by nonzero perpendicular displacement of the frame vertices (figure 8), reduced validity by causing frame misalignment leading to blurred images, thereby limiting reliable fascicle identification. Together, these limitations induce uncertainties and should be considered when interpreting results. Nonetheless, the relaxed fascicle lengths (table 3) correspond to literature. Cadaveric studies describe m. rectus femoris fascicles of 66 mm (Wickiewicz et al., 1988) and OFL of 78 mm (Horsman et al., 2006; Ward et al., 2008). Because the present measurements were taken with the knee fully extended, shorter fascicle lengths could be expected, whereas relaxed fascicles are generally longer. Therefore, the expected length in this posture is difficult to define. Nevertheless, the correspondence with literature indicates that the measurements fall within a physiologically plausible range, supporting the validity of the relaxed fascicle length estimates.

Within the proposed methodology it as assumed that the angle-specific relaxed fascicle length and active fascicle length could be estimated from distal aponeurosis displacement. However, the 2D reconstruction of the m. rectus femoris demonstrated substantial architectural complexity, as both fascicle length and pennation angle vary throughout the muscle (figure 9 and table 3). This complexity challenges the underlying assumption of the proposed method to estimates angle-specific and active fascicle length by adding or subtracting distal aponeurosis displacement from the relaxed fascicle length. Because the fascicles are oriented obliquely relative to the muscle's line of action, varying throughout the muscle and with activation level, the aponeurosis displacement does not correspond directly to true fascicle length changes. As a result, this approach does not provide valid estimates of active fascicle length. Given this limitation, alternative ultrasound techniques may be more suitable. Three-dimensional reconstruction would better capture the complex muscle architecture and allow improved estimation of fascicle lengths along the entire m. rectus femoris (e.g., Weide et al., 2017), although this approach still requires estimation of shortening during activation. An alternative that avoids this requirement is to increase the imaging field, providing a wider view of the muscle during activation. This allows more accurate estimation of pennation angle throughout the muscle and enables derivation of fascicle length from muscle thickness. Such measurements can be achieved using extended field-of-view ultrasound and multiprobe integration techniques. (e.g. Noorkoiv et al.,2008; Sahinis et al., 2020; Johnson et al., 2021). These methods remain easily accessible and are therefore suitable for application on larger populations.

The small sample size may limit the generalizability of the findings. However, it was sufficient to demonstrate the invalidity of the proposed in vivo methodology for measuring OFL. Substantial methodological improvements, as outlined above, are required before further measurements are appropriate. To further assess the feasibility of the proposed methodology, future studies should apply it to muscles and joints that do not require a leg rest, allowing more reliable joint-moment measurements, and exhibit less complex muscle architecture for more accurate fascicle length estimation.

4. Conclusion

This study evaluated the validity of an in vivo methodology for estimating OFL. The findings demonstrate that the current approach does not provide valid OFL estimates, primarily due to unreliable joint moment measurements and invalid assumptions regarding fascicle behaviour during activation. Although electrical stimulation proved feasible and relaxed fascicle lengths were measured reliably, active fascicle lengths could not be derived from aponeurosis displacement because of the muscle's complex architecture.

These findings provide insight into the challenges of developing reliable in vivo methodologies for measuring OFL. They demonstrate that accurate knee joint-moment estimation is difficult when relying solely on a loadcell and motion capture. Furthermore, the results highlight that valid fascicle length measurements are inherently challenging due to the complex architecture of in vivo muscles and the reliance on simplifying assumptions. Collectively, these results emphasize that accurate determination of OFL requires methodologies that account for both mechanical and anatomical complexities.

Recommendations for future work are (1) apply the developed methodology to other muscles and joints that do not require a leg rest and exhibit less complex muscle architecture, (2) investigate the possibility of increasing the electrical muscle stimulation without inducing fatigue, (3) explore methods for measuring knee moment without a leg-rest, for instance a dynamometer, and (4) use more advanced ultrasound techniques for better estimation of fascicle length. Ultimately, these insights will provide a foundation for in vivo estimation of OFL, facilitating investigation of population-specific differences and improving diversity in musculoskeletal modelling.

References

Abbott B. C., Aubert, X. M., The force exerted by active striated muscle during and after change of length. J Physiol. 1952; 117:77–86. PMID: 14946730

Adkins, A. N., Dewald, J. P. A., Garmirian, L. P., Nelson, C. M., & Murray, W. M. (2021). Serial sarcomere number is substantially decreased within the paretic biceps brachii in individuals with chronic hemiparetic stroke. *Proceedings Of The National Academy Of Sciences*, *118*(26). https://doi.org/10.1073/pnas.2008597118

Brand, R. A., Pedersen, D. R., & Friederich, J. A. (1986). The sensitivity of muscle force predictions to changes in physiologic cross-sectional area. *Journal Of Biomechanics*, *19*(8), 589–596. https://doi.org/10.1016/0021-9290(86)90164-8

Charles, J. P., Suntaxi, F., & Anderst, W. J. (2019). In vivo human lower limb muscle architecture dataset obtained using diffusion tensor imaging. *PLoS ONE*, *14*(10), e0223531. https://doi.org/10.1371/journal.pone.0223531

Chen, X., Sanchez, G. N., Schnitzer, M. J., & Delp, S. L. (2016). *Changes in sarcomere lengths of the human vastus lateralis muscle with knee flexion measured using in vivo microendoscopy. Journal of Biomechanics, 49*(13), 2989–2994. https://doi.org/10.1016/j.jbiomech.2016.07.013

Chen, Z., & Franklin, D. W. (2025). Muscle Moment Arm–Joint Angle Relations in the Hip, Knee, and Ankle: A Visualization of Datasets. *Annals Of Biomedical Engineering*. https://doi.org/10.1007/s10439-025-03735-w

Cromie, M. J., Sanchez, G. N., Schnitzer, M. J., & Delp, S. L. (2012). Sarcomere lengths in human extensor carpi radialis brevis measured by microendoscopy. *Muscle & Nerve*, *48*(2), 286–292. https://doi.org/10.1002/mus.23760

Damsgaard, M., Rasmussen, J., Christensen, S. T., Surma, E., & De Zee, M. (2006). Analysis of musculoskeletal systems in the AnyBody Modeling System. *Simulation Modelling Practice And Theory*, *14*(8), 1100–1111. https://doi.org/10.1016/j.simpat.2006.09.001

Delp, S. L., Anderson, F. C., Arnold, A. S., Loan, P., Habib, A., John, C. T., Guendelman, E., & Thelen, D. G. (2007). OpenSim: Open-Source Software to Create and Analyze Dynamic Simulations of Movement. *IEEE Transactions On Biomedical Engineering*, *54*(11), 1940–1950. https://doi.org/10.1109/tbme.2007.901024

De Groote, F., Van Campen, A., Jonkers, I., & De Schutter, J. (2010). Sensitivity of dynamic simulations of gait and dynamometer experiments to hill muscle model parameters of knee flexors and extensors. *Journal Of Biomechanics*, *43*(10), 1876–1883. https://doi.org/10.1016/j.jbiomech.2010.03.022

De Ruiter, C. J., Kooistra, R. D., Paalman, M. I., & De Haan, A. (2004). Initial phase of maximal voluntary and electrically stimulated knee extension torque development at different knee angles. *Journal Of Applied Physiology*, *97*(5), 1693–1701. https://doi.org/10.1152/japplphysiol.00230.2004

Friederich, J. A., & Brand, R. A. (1990). Muscle fiber architecture in the human lower limb. *Journal Of Biomechanics*, *23*(1), 91–95. https://doi.org/10.1016/0021-9290(90)90373-b

Hoffman, B.W., Lichtwark, G.A., Carroll, T.J., Cresswell, A.G., (2012). A comparison of two Hill-type skeletal muscle models on the construction of medial gastrocnemius lengthtension curves in humans in vivo. J. Appl. Physiol. 1985 (113), 90–96. https://doi.org/10.1152/japplphysiol.00070.2012

Horsman, M. K., Koopman, H., Van Der Helm, F., Prosé, L. P., & Veeger, H. (2006). Morphological muscle and joint parameters for musculoskeletal modelling of the lower extremity. *Clinical Biomechanics*, *22*(2), 239–247. https://doi.org/10.1016/j.clinbiomech.2006.10.003

Johnson, A. W., Adams, L., Kho, J. B., Green, D. M., Pace, N. B., & Mitchell, U. H. (2021). Extended field-of-view ultrasound imaging is reliable for measuring Transversus Abdominis muscle size at rest and during contraction. *BMC Musculoskeletal Disorders*, *22*(1), 282. https://doi.org/10.1186/s12891-021-04157-0

Kukić, F., Mrdaković, V., Stanković, A., & Ilić, D. (2022). Effects of Knee Extension Joint Angle on Quadriceps Femoris Muscle Activation and Exerted Torque in Maximal Voluntary Isometric Contraction. *Biology*, *11*(10), 1490. https://doi.org/10.3390/biology11101490

Lichtwark, G. A., Farris, D. J., Chen, X., Hodges, P. W., & Delp, S. L. (2018). *Microendoscopy reveals positive correlation in multiscale length changes and variable sarcomere lengths across different regions of human muscle. Journal of Applied Physiology, 125*(6), 1812–1820. https://doi.org/10.1152/japplphysiol.00480.2018

Lieber, R. L., Loren, G. J., & Friden, J. (1994). In vivo measurement of human wrist extensor muscle sarcomere length changes. *Journal Of Neurophysiology*, *71*(3), 874–881. https://doi.org/10.1152/jn.1994.71.3.874

Luis, I., Afschrift, M., De Groote, F., & Gutierrez-Farewik, E. M. (2022). Evaluation of musculoskeletal models, scaling methods, and performance criteria for estimating muscle excitations and fiber lengths across walking speeds. *Frontiers in Bioengineering And Biotechnology*, *10*. https://doi.org/10.3389/fbioe.2022.1002731

Maganaris, C.N., 2001. Force-length characteristics of in vivo human skeletal muscle. Acta Physiol. Scand. 172, 279–285. https://doi.org/10.1046/j.1365- 201x.2001.00799.x

Marginson, V., & Eston, R. (2001). The relationship between torque and joint angle during knee extension in boys and men. *Journal Of Sports Sciences*, *19*(11), 875–880. https://doi.org/10.1080/026404101753113822

Mornas, A., Hollville, E., Brocherie, F., Derouck, T., Racinais, S., & Guilhem, G. (2024b). Test-retest reliability of gastrocnemius medialis fascicle force-length relationship. *Journal Of Biomechanics*, *171*, 112170. https://doi.org/10.1016/j.jbiomech.2024.112170

Nikolaidou, M.E., Marzilger, R., Bohm, S., Mersmann, F., Arampatzis, A., 2017. Operating length and velocity of human M. vastus lateralis fascicles during vertical jumping. R. Soc. Open Sci. 4, 170185 https://doi.org/10.1098/rsos.170185

Noorkoiv, M., Stavnsbo, A., Aagaard, P., & Blazevich, A. J. (2010). In vivo assessment of muscle fascicle length by extended field-of-view ultrasonography. *Journal Of Applied Physiology*, *109*(6), 1974–1979. https://doi.org/10.1152/japplphysiol.00657.2010

Pandy, M. G., & Zajac, F. E. (1991b). Optimal muscular coordination strategies for jumping. *Journal Of Biomechanics*, *24*(1), 1–10. https://doi.org/10.1016/0021-9290(91)90321-d

Redl, C., Gfoehler, M., & Pandy, M. G. (2007). Sensitivity of muscle force estimates to variations in muscle–tendon properties. *Human Movement Science*, *26*(2), 306–319. https://doi.org/10.1016/j.humov.2007.01.008

Sahinis, C., Kellis, E., Galanis, N., Dafkou, K., & Ellinoudis, A. (2020). Intra- and inter-muscular differences in the cross-sectional area of the quadriceps muscles assessed by extended field-of-view ultrasonography. *Medical Ultrasonography*, *22*(2), 152. https://doi.org/10.11152/mu2302

Scovil, C. Y., & Ronsky, J. L. (2005). Sensitivity of a Hill-based muscle model to perturbations in model parameters. *Journal Of Biomechanics*, *39*(11), 2055–2063. https://doi.org/10.1016/j.jbiomech.2005.06.005

SENIAM. (n.d.). http://seniam.org/

Van Soest, A. J., & Bobbert, M. F. (1993). The contribution of muscle properties in the control of explosive movements. *Biological Cybernetics*, *69*(3), 195 204. https://doi.org/10.1007/bf00198959

Wakeling, J. M., Febrer-Nafría, M., & De Groote, F. (2023). A review of the efforts to develop muscle and musculoskeletal models for biomechanics in the last 50 years. *Journal Of Biomechanics*, *155*, 111657. https://doi.org/10.1016/j.jbiomech.2023.111657

Walker, S. M., & Schrodt, G. R. (1974). I segment lengths and thin filament periods in skeletal muscle fibers of the rhesus monkey and the human. *The Anatomical Record*, *178*(1), 63–81. https://doi.org/10.1002/ar.1091780107

Ward, S.R., Smallwood, L.H., Lieber, R.L., 2005. Scaling of human lower extremity muscle architecture to skeletal dimensions. In: ISB XXth Congress. Cleveland, Ohio.

Ward, S.R., Kingsbury, T., Winters, T., Lieber, K.M., Braun, J., Eng, C.M., Lieber, R.L., 2007. In: Scaling of Joint Mechanics and Muscle Architecture in the Human Knee, American Society of Biomechanics Meeting, Stanford University, California.

Ward, S. R., Eng, C. M., Smallwood, L. H., & Lieber, R. L. (2008). Are Current Measurements of Lower Extremity Muscle Architecture Accurate? *Clinical Orthopaedics And Related Research*, *467*(4), 1074–1082. https://doi.org/10.1007/s11999-008-0594-8

Weide, G., Van Der Zwaard, S., Huijing, P. A., Jaspers, R. T., & Harlaar, J. (2017). 3D Ultrasound Imaging: Fast and Cost-effective Morphometry of Musculoskeletal Tissue. *Journal Of Visualized Experiments*, *129*. https://doi.org/10.3791/55943

Wickiewicz, T. L., Roy, R. R., Powell, P. L., & Edgerton, V. R. (1983). Muscle Architecture of the Human Lower Limb. *Clinical Orthopaedics And Related Research*, *179*(179), 275–283. https://doi.org/10.1097/00003086-198310000-00042

Young, K. W., Kuo, B. P., O'Connor, S. M., Radic, S., & Lieber, R. L. (2017). In Vivo Sarcomere Length Measurement in Whole Muscles during Passive Stretch and Twitch Contractions. *Biophysical Journal*, *112*(4), 805–812. https://doi.org/10.1016/j.bpj.2016.12.046

Yu, B., & Herzog, W. (2023). In vivo vastus lateralis fascicle excursion during speed skating imitation. *Journal Of Biomechanics*, *160*, 111814. https://doi.org/10.1016/j.jbiomech.2023.111814

Appendix I – Selection of Anatomical Landmark Tracking Point for the Excursion Method

To determine the optimal tracking point for estimating muscle-tendon-unit length change using the excursion method, three anatomical landmarks were evaluated: the patella, ligamentum patellae, and tibial tuberosity. Figure I.1 presents the resulting muscle-tendon-unit length changes and corresponding muscle-tendon moment arms as functions of knee angle for each landmark. Compared with literature values, tracking the lig. patellae showed the closest correspondence with published data (Chen and Franklin, 2025). In contrast, tracking the tuberositas tibiae and apex patellae resulted in systematic over- and underestimation of muscle-tendon unit length changes and corresponding moment arms. Accordingly, the lig. patellae was selected as the anatomical reference for m. rectus femoris muscle-tendon moment-arm estimation.

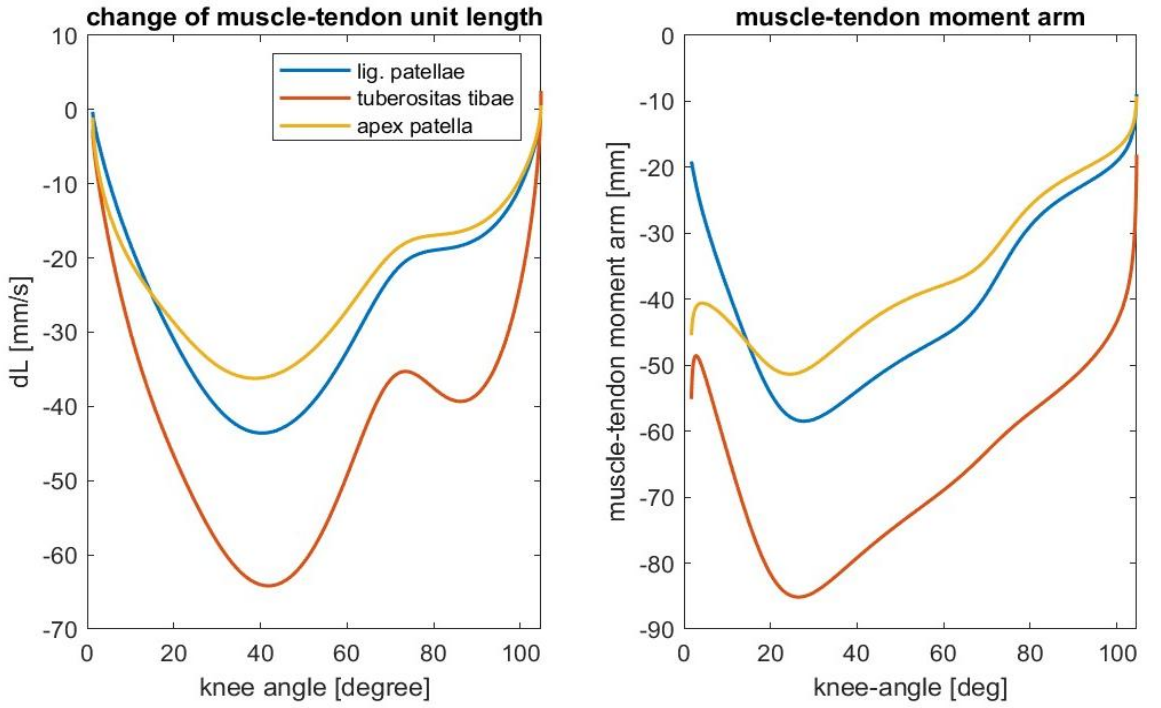

Figure I.1. Data from participant A (extension 1). (a) Change in muscle-tendon unit length as a function of knee angle. (b) Corresponding muscle-tendon moment arms as a function of knee angle for the three tracked anatomical landmarks. One measurement is shown as representative, as all measurements exhibited this trend.

Appendix II – Calculation of Knee Angle

The knee angle (φ_{knee}) is calculated as the angle between two vectors representing the thigh and shank. The vectors were defined using the positions of the anatomical landmarks relative to the clusters of reflective makers during a measurement.

Abbreviations of anatomical landmarks	
trochanter major	TM
lateral femoral epicondyle	LFE
medial femoral epicondyle	MFE
lateral malleolus	LM
medial malleolus	MM

Table II.1: abbreviations of anatomical landmarks

The position vectors to the knee and ankle centre are calculated as the midpoint of the two vector to the femoral epicondyles and malleoli:

$$\bar{r}_{kneecentre} = \frac{(\bar{r}_{LFE}+\bar{r}_{MFE})}{2} \quad \text{(II.1)}$$

$$\bar{r}_{anklecentre} = \frac{(\bar{r}_{LM}+\bar{r}_{MM})}{2} \quad \text{(II.2)}$$

In which $\bar{r}$ denotes a position vector, abbreviations are explained in table (II.1). The vector representing the shank is calculated as the vector from knee-centre to ankle-centre

$$\bar{r}_{shank} = \bar{r}_{anklecentre} - \bar{r}_{kneecentre} \quad \text{(II.3)}$$

In which $\bar{r}_{shank}$ represents the shank vector.

The thigh vector is calculated from the knee centre to the femoral head.

$$\bar{r}_{thigh} = \bar{r}_{femoralhead} - \bar{r}_{kneecentre} \quad \text{(II.4)}$$

Where $\bar{r}_{thigh}$ denotes the thigh vector and $\bar{r}_{femoralhead}$ the position vector of the femoral head. $\bar{r}_{femoralhead}$ had to be estimated based on the position of TM and known knee angle. $\bar{r}_{femoralhead}$ could be calculated as:

$$\bar{r}_{femoralhead} = (\bar{r}_{TM} - \bar{r}_{kneecentre}) + \bar{d} \quad \text{(II.5)}$$

In which $\bar{d}$ denotes the correction vector from TM to femoral head. It was assumed that when the knee was fully extended, the angle between $\bar{r}_{thigh}$ and $\bar{r}_{shank}$ would be 180°. From this $\bar{d}$ could be derived as:

$$\bar{d} = -\bar{r}_{shank_{180°}} - (\bar{r}_{TM} - \bar{r}_{kneecentre})_{\,180°} \quad \text{(II.6)}$$

In which $-\bar{r}_{shank_{180°}}$ is the shank vector but 180° rotated when the knee was fully extended, $(\bar{r}_{TM} - \bar{r}_{kneecentre})_{\,180°}$ represents a vector from knee centre to TM when the knee was fully extended. $\bar{d}$ is then used from every measurement to estimate the position of the femoral head. The knee angle is calculated with the inner product rule:

$$\varphi_{knee} = \cos^{-1}\left(\frac{\bar{r}_{thigh}\cdot\bar{r}_{shank}}{\|\bar{r}_{thigh}\|\cdot\|\bar{r}_{shank}\|}\right) \quad \text{(II.7)}$$

Where φ_{knee} represents the knee angle and ||_|| denotes the norm of a vector.

Appendix III – Calculation of Knee Moment

The knee moment was calculated using the free body diagram (figure III.1) and the moment-equation of the shank, see equation III.1.

$$\sum \bar{M} = \bar{M}_{knee} + \bar{M}_{cord} + \bar{M}_{gravity} = 0 \quad \text{(III.1)}$$

Where $\sum \bar{M}$ denotes the sum of all moments on the shank, $\bar{M}_{knee}$the total knee moment, $\bar{M}_{cord}$ the external moment from the cord and $\bar{M}_{gravity}$ the external moment from gravity. The norm of the knee moment is used to calculate the muscle force and is calculated with equation III.2, in which ||_|| denotes the norm of the vector.

$$\|\bar{M}_{knee}\| = \left\|\bar{M}_{cord} + \bar{M}_{gravity}\right\| \quad \text{(III.2)}$$

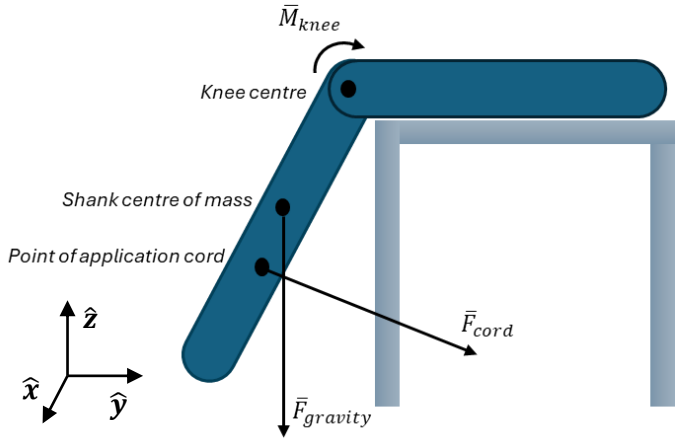

Figure III.1: Free body diagram of the shank. $\bar{F}_{cord}$ represents the external force from cord on shank, $\bar{F}_{gravity}$ represents the external gravity force on shank moments, $\bar{M}_{knee}$ represents the total knee moment, the centre of rotation is the knee centre. The right-handed coordinate system has the positive z-axis pointing upward.

The knee-centre was defined as the midway between the lateral and medial femoral epicondyle. $\bar{M}_{cord}$ was calculated as the cross product of the moment arm from point of application to the knee-centre and the cord force vector,

$$\bar{M}_{cord} = (\bar{r}_{PoA} - \bar{r}_{kneecentre}) \times \bar{F}_{cord} \quad \text{(III.3)}$$

in which $\bar{r}_{PoA}$ represents the vector to the point of application, $\bar{r}_{kneecentre}$ the vector to the knee-center and $\bar{F}_{cord}$ the cord force vector. $\bar{F}_{cord}$ was calculated as the product of the measured force from the loadcell and the direction of the cord, obtained from the markers on the point of application and cord, see experimental setup.

$$\bar{F}_{cord} = F_{cord} \cdot \frac{\bar{r}_{cord} - \bar{r}_{PoA}}{\|\bar{r}_{cord} - \bar{r}_{PoA}\|} \quad \text{(III.4)}$$

where F_{cord} denotes the measured force and $\bar{r}_{cord}$ the position vector to the maker on the cord. $\bar{M}_{gravity}$ was calculated similarly as

$$\bar{M}_{gravity} = (\bar{r}_{CoM} - \bar{r}_{kneecentre}) \times \bar{F}_{gravity} \quad \text{(III.5)}$$

where $\bar{r}_{CoM}$ represents shank centre of mass vector and $\bar{F}_{gravity}$ the gravitational force vector that was calculate as,

$$\bar{F}_{gravity} = m_{shank} \cdot \bar{g} \quad \text{(III.6)}$$

in which m_{shank} and $\bar{g}$ denote the shank mass and gravitational acceleration of -9.81 m/s^2 in the z-direction (figure III.1). m_{shank} and $\bar{r}_{CoM}$ were calculated with respect to knee centre using a regression function based on shank length, body weight, and sex from De Leva (1996). They corrected data from Zatsiorski et al. (1990a), which included college aged, Caucasian males and females.